Progress in Nuclear Energy 142 (2021) 103998

Contents lists available at ScienceDirect

Progress in Nuclear Energy

journal homepage: www.elsevier.com/locate/pnucene

APERTRACK: A particle-tracking model to simulate radionuclide transport in the Arabian/Persian Gulf

R. Periáñez

Dpt Física Aplicada I, ETSIA, Universidad de Sevilla, Ctra Utrera km 1, 41013 Sevilla, Spain

ARTICLE INFO

Keywords:
Arabian/Persian Gulf
Tide
Baroclinic circulation
Radionuclide
Transport
Sediment

ABSTRACT

A Lagrangian rapid-response model for simulating the transport of radionuclides in the Arabian (or Persian) Gulf is described. The model is based on a tide model including five constituents, which was solved in advance, and baroclinic circulation was obtained from HYCOM operational ocean model. The radionuclide model includes physical transport (advection and diffusion), radioactive decay and geochemical processes (interactions of radionuclides between water and sediments, described in a dynamic way). The model can lead with instantaneous or continuous releases. Some hypothetical releases from a coastal nuclear power plant were simulated. Results show that the moment of release affects the fate of radionuclides due to the temporal variability of baroclinic currents. Also, comparing results for releases of Cs and Pu, it was seen how the geochemical behaviour of the radionuclide clearly affects the further radionuclide distributions. It is easy to setup the model for a particular release and it provides a fast response; thus the present model is an appropriate tool to support decision-making after a nuclear accident.

1. Introduction

The Arabian (or Persian) Gulf, from now on APG, is a shallow water body with a mean depth of 36 m (Alosairi and Pokavanich, 2017). It is connected to the Gulf of Oman (Indian Ocean) through the Strait of Hormuz, thus it is a semi-enclosed marginal sea (Fig. 1). Countries which surround the APG are the United Arab Emirates, Saudi Arabia, Qatar, Bahrain (which consists of more than 30 islands in the APG), Kuwait, Iraq and Iran (this last in the eastern side).

Circulation in the APG is forced by both winds and thermohaline (density driven) forcing. Given the excess of evaporation over precipitation and river inflow, a inverse estuarine circulation results; with the high salinity waters leaving the APG through a deep layer of the Strait of Hormuz and being replaced by a fresher surface inflow from the Indian Ocean (Kämpf and Sadrinasab, 2006). This inflow occurs along the Iranian coast (Johns et al., 2003). Tides in the Gulf form standing waves, being dominant the semidiurnal and diurnal tides. The dimensions of the Gulf lead to a resonance of both tides, with one amphidromic point in the case of the diurnal and two in the case of the semidiurnal ones (Hyder et al., 2013).

Desalination plants are the main freshwater source to the APG countries (Alosairi and Pokavanich, 2017). For instance, in Abu Dhabi in 2007 desalination plants produced more than 2.3 million cubic metre of fresh water per day, which accounted for 36% of the total water production (Environmental Agency Abu Dhabi, 2009) in such country. In addition, commercial and subsistence fisheries provide a living for a large sector of the coastal population (Abdi et al., 2006).

The coastal environment of the APG has been exposed to various sources of radioactive pollution (Al-Ghamdi et al., 2016), including desalination plants (which are the main source of radium in the brine discharged to the sea) and phosphate industry (radium in phosphogypsum waste). Oil spills are relatively common in the APG, in addition to the massive oil releases during the 1991 Gulf War, which have both added natural radionuclides into the local marine environment. A review on radioactivity levels in the APG may be seen in Uddin et al. (2020).

In addition to what it is commented above, the APG, Strait of Hormuz and Gulf of Oman are one of the most important waterways in the world, thus exposed to pollution incidents due to shipping activities (mainly potential oil spills). But recently, there has been concern about the nuclear power plants which are now operating along the APG coasts (Kamyab et al., 2018). There are two operational NPPs in the region, Bushehr in Iran and Barakah in UAE, whose unit 1 was connected to the power grid in summer 2020. About seventeen more are planned in the Kingdom of Saudi Arabia, with the intention that they are operational by 2030 (Uddin et al., 2020).

Consequently, it is relevant to have a numerical model able to assess the effects of radioactive releases into the APG from such NPPs (or from a ship transporting nuclear wastes for instance). Discharges could

E-mail address: rperianez@us.es.

https://doi.org/10.1016/j.pnucene.2021.103998
Received 17 February 2021; Received in revised form 5 October 2021; Accepted 8 October 2021

Table 1
Model availability.

Program name	APERTRACK
Developer	R. Periáñez, University of Sevilla
Contact	rperianez@us.es
Hardware	Desktop PC
Program code	Fortran
Cost	Free
Availability	https://personal.us.es/rperianez/

be due to the normal operation of the plants or to acute accidental releases. A significant conclusion from IAEA (International Atomic Energy Agency) MODARIA and MODARIA-II (Modelling and Data for Radiological Impact Assessments) programmes (Periáñez et al., 2019a, 2016a; IAEA, 2019) was the need to have site specific models which are carefully adapted to the region and made available for any marine area potentially exposed to a radionuclide release. This would help the decision-making process after an accident. Recent studies describing marine radionuclide transport models applied to other areas potentially exposed to nuclear accidents are, for instance, those of Periáñez et al. (2021) for the northern Indian Ocean and Tsabaris et al. (2021) for the eastern Mediterranean Sea. A review of models applied to simulate Fukushima releases in the Pacific Ocean may be seen in Periáñez et al. (2019a).

Some models are described in literature concerning the dispersion of oil spills in the APG (Proctor et al., 1994; Faghihifard and Badri, 2016; Al-Rabeh et al., 2000); however this is not the case with radionuclides. A radionuclide transport modelling work for the APG which could be found is that of Kamyab et al. (2018). These authors applied CROM[1] model to simulate a hypothetical accident at Bushehr NPP; but CROM is essentially a Gaussian model based on the generic models described in IAEA (2001) suitable for steady conditions at a local scale, not able to deal with spatio-temporal variations of currents due to tidal oscillations and thermohaline forcing, thus its applicability in this case is questionable. Hassanvand and Mirnejad (2019) calculate tides in the northern APG and describe their effects in transporting radionuclides released from Bushehr in a qualitative way (without applying a transport model). They again use CROM to estimate transport and doses. The purpose of this paper is to fill such gap, presenting a radionuclide transport model for the APG which could be used for both chronic and accidental releases, including realistic descriptions of tidal and baroclinic currents, and finally including interactions of radionuclides between water and sediments; in line with recommendations in IAEA (2019). Moreover, the model is able to provide a fast response, thus it would be useful to support the decision-making process after an accident. Availability of the model is summarized in Table 1.

The model is described in Section 2, where hydrodynamic methods (for tides and baroclinic circulation) and radionuclide transport description are presented separately. Results are presented in Section 3; first results of the tidal and baroclinic models are described (Section 3.1). Next some examples of simulations of radionuclide releases in the APG are presented (Section 3.2).

2. Model description

2.1. Tidal modelling

A two dimensional depth-averaged model was used to simulate tides in the APG. Calculated elevations and currents are treated through standard tidal analysis (Pugh, 1987, Chapter 4) and tidal constants (amplitudes and phases) are then calculated and stored for each grid cell in the computational domain. Five constituents were considered: three semidiurnal (M_2, S_2 and N_2) and two diurnal (K_1 and O_1). Tidal model equations (see for instance Periáñez, 2012; a summary is presented in Appendix A) are solved for each constituent and tidal analysis is carried out for each constituent as well. The Eulerian residual transport is calculated, according to the procedure described in Periáñez (2012) and summarized in Appendix A, to obtain tidal residual currents. Boundary conditions to solve the equations consist of specifying water surface elevations and phases, from measured tidal constants, along the open boundaries of the domain. Measurements were obtained from Pous et al. (2012). The model domain extends from 47° E to 57° E in longitude and from 23° N to 31° N in latitude (Fig. 1). Resolution is the same as HYCOM model, 0.08° (see Section 2.2).

Once that amplitudes and phases (adapted phase, i.e., for the local time meridian) for each grid cell and constituent (calculated from the tidal analysis) are known, the tidal prediction equation is used to evaluate the exact tidal state during each time step of the radionuclide simulation and location in the APG. The procedure is described in Parker (2007) and Boon (2011) and summarized in Appendix A.

The tidal model is two-dimensional, thus it provides averaged currents over the water column. A three-dimensional current field is generated using a standard current profile, since currents decrease from sea surface to the bottom because of friction. Details may be seen in Pugh (1987) and Periáñez and Pascual-Granged (2008).

The present tidal model was successfully tested for several regions at quite different spatial scales (Periáñez, 2007, 2009, 2012; Periáñez et al., 2013; Periáñez and Abril, 2014; Periáñez, 2020a).

2.2. Baroclinic circulation

HYCOM (Hybrid Coordinate Ocean Model, (Bleck, 2001)) model was used to obtain baroclinic circulation in the APG. HYCOM is a primitive equation general circulation model with 40 vertical layers increasing in thickness from the surface to the sea bottom and 0.08° horizontal resolution in both latitude and longitude. Examples of HYCOM model applications over the world are presented in the model web page (https://www.hycom.org/). Actually, this model has already been used to study circulation in the APG (Yao and Johns, 2010a,b). Daily currents were downloaded from HYCOM data server for the APG (the same domain specified above for the tidal model). Note that the tidal model is required since tides are not included in HYCOM.

2.3. Radionuclide transport

The model is Lagrangian as commented before, thus the radionuclide release into the sea is simulated by means of a number of particles. Each particle is equivalent to a number of units (for instance Bq), and trajectories are calculated during the simulated period. The transport model considers physical transport (advection due to water currents and mixing due to turbulence) plus radioactive decay and interactions of radionuclides with bed sediments (adsorption/desorption reactions). Radionuclide concentrations are obtained from the number of particles within each grid cell and compartment (surface water, deep water and sediment as explained in Appendix B) and the number of units (Bq) which corresponds to each particle.

Turbulent mixing, radioactive decay and exchanges of radionuclides between water and sediment are described through a stochastic method (Periáñez and Elliott, 2002; Kobayashi et al., 2007; Periáñez et al., 2019a). A dynamic method is applied to describe water/sediment interactions, thus a kinetic coefficient k_1 describes the transfer of radionuclides from water to sediment and a coefficient k_2 governs the inverse process. A summary of the involved equations may be seen in Appendix B. As in other works, k_1 is derived from the radionuclide equilibrium distribution coefficient k_d (provided for instance in (IAEA, 2004)) and a standard experimental value for k_2 (Periáñez, 2009; Periáñez et al., 2013, 2016b). Equations are summarized in Appendix B.

[1] ftp://ftp.ciemat.es/pub/CROM.

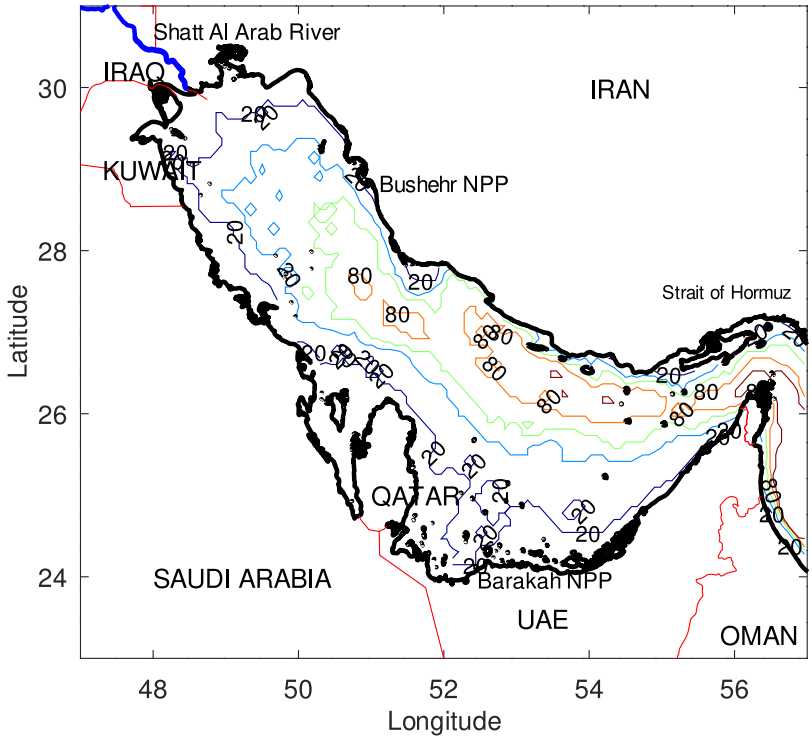

Fig. 1. Map of the APG, which corresponds to the present model domain. Isobaths of 20, 40, 60, 80 and 100 m are drawn. The locations of Bushehr and Barakah NPPs are also shown.

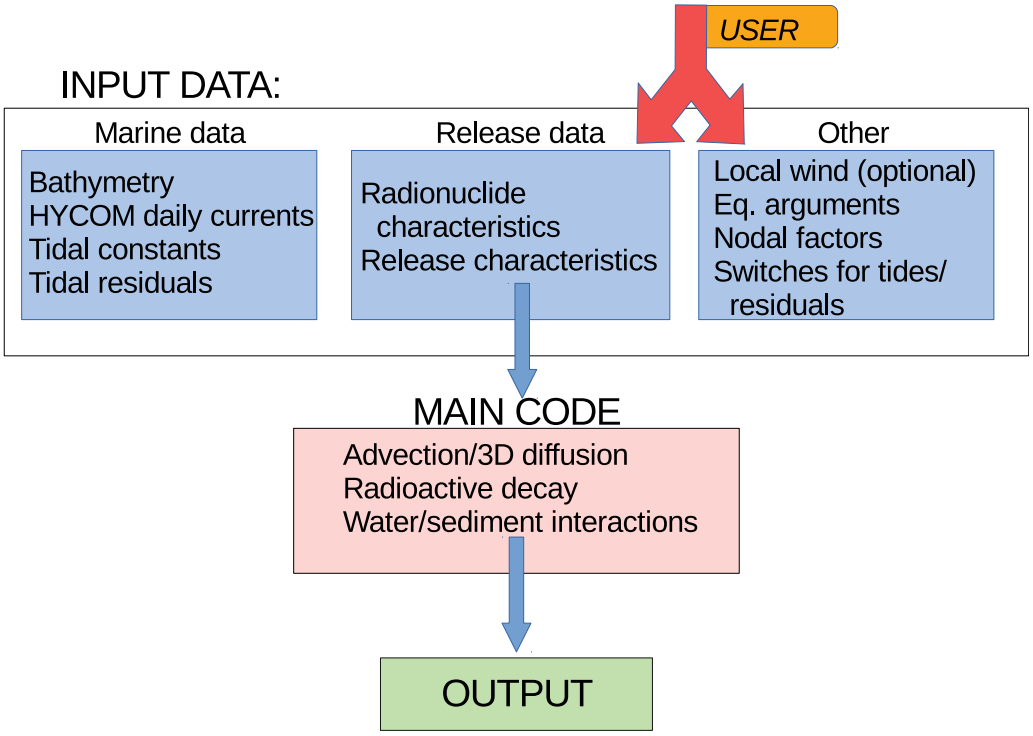

Fig. 2. General scheme of the modelling procedure. The user must specify only *release data* and *other*. Equilibrium arguments and nodal factors for year 2021 are set as default option.

2.4. Model input

A number of files specify the release characteristics (date, time, position in geographic coordinates, depth, magnitude and duration) and simulation time, radionuclide properties (decay constant and equilibrium distribution coefficient (which may be obtained from IAEA (2004) as mentioned above), and, finally, an optional wind forecast (see next paragraph) and components of the currents to be used: tidal currents and residuals may be individually switched on and off (to

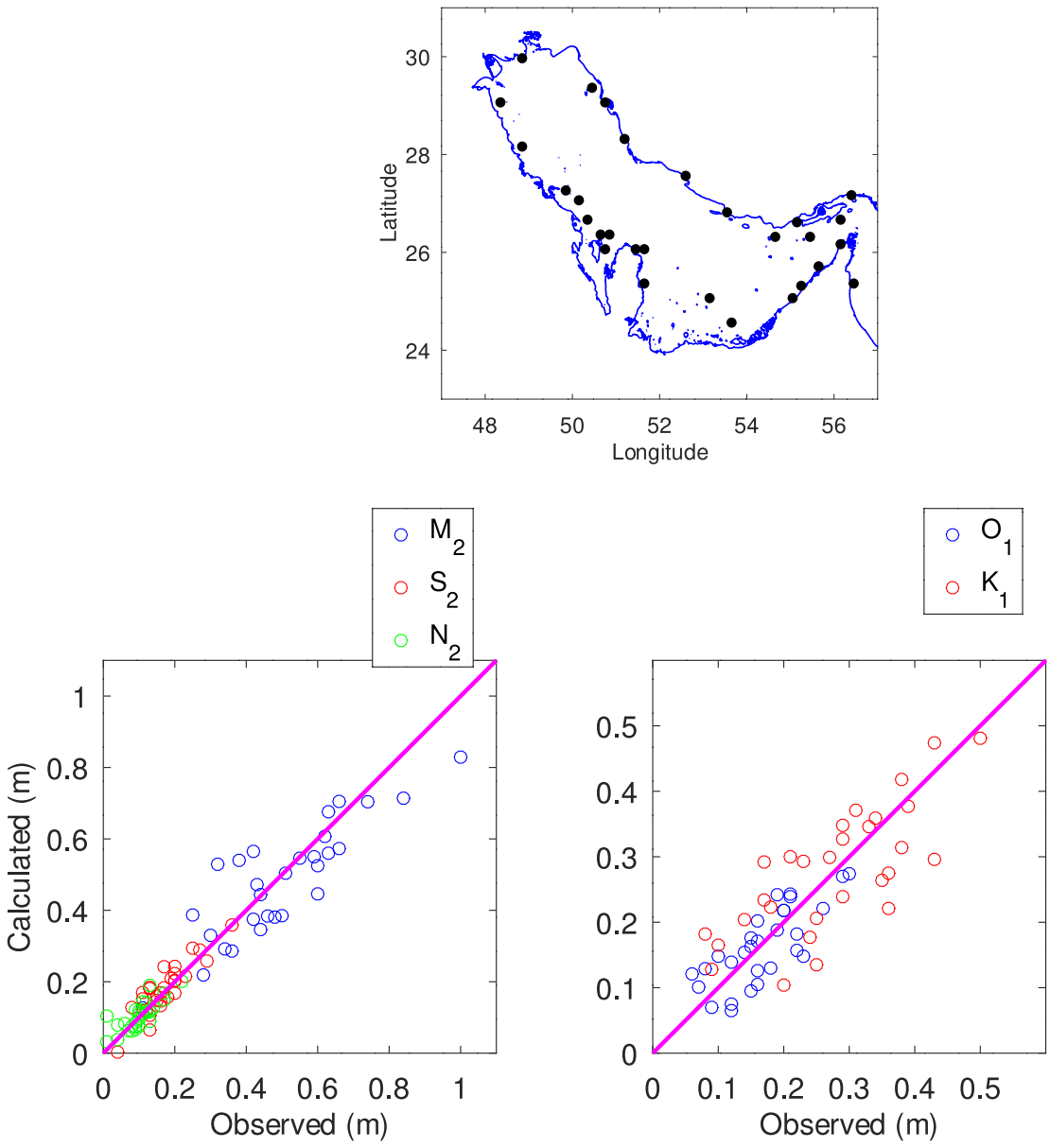

Fig. 3. Comparison between calculated and observed amplitudes for the semidiurnal (left) and diurnal (right) constituents considered in the model. The map in the top shows points where tidal constants were measured (black dots).

allow comparisons if they are included or not in the simulations or to speed them up by removing tides in the calculations). These switches are provided in a specific file named `input.dat`. The file `tide-data.dat` contains equilibrium arguments and nodal factors of the 5 tidal constituents for year 2021, set as default, as explained in Appendix A. Thus, this file should be modified only if a simulation for a different year is to be carried out. Equilibrium arguments and nodal factors for the corresponding year should then be used. A list of the input files which should be modified for a particular simulation is given in Table 2.

In the case of a simulation to assess the effects of an acute release due to an accident, for instance, it may be relevant to include a local wind, which is considered uniform in the release area. Wind data are provided in a file as a number of different "wind episodes" (any number can be used with a maximum of 100), each one characterized by a wind speed, direction and start and end times measured in hours after the pollutant release beginning. This time-evolving wind conditions may be obtained from weather forecasts. It should be commented that HYCOM calculations already include atmospheric forcing. However, the present definition of "wind episodes" gives the opportunity of describing transport in case that an accident occurs, for instance, during a local storm which is not described in HYCOM. The need of adding this local wind in some oil spill simulations in the Red Sea was clearly shown in Periáñez (2020a) and was also used in a radionuclide transport model for the same sea (Periáñez, 2020b). The wind-induced current is considered to decrease logarithmically to zero from the surface. The mathematical form of this profile may be seen in Pugh (1987), for instance. It should be clearly pointed out that using this "local wind" is

Table 2
Input files which must be modified for each specific simulation. It is required to modify `tide-data.dat` only if a simulation for other year than 2021 is to be carried out.

`tide-data.dat`	Equilibrium arguments and nodal factors
`release.dat`	Release data and simulation time
`RN.dat`	Contaminant properties (decay constant and k_d)
`input.dat`	Switches to include or not tidal circulation
`wind.dat`	Local wind data

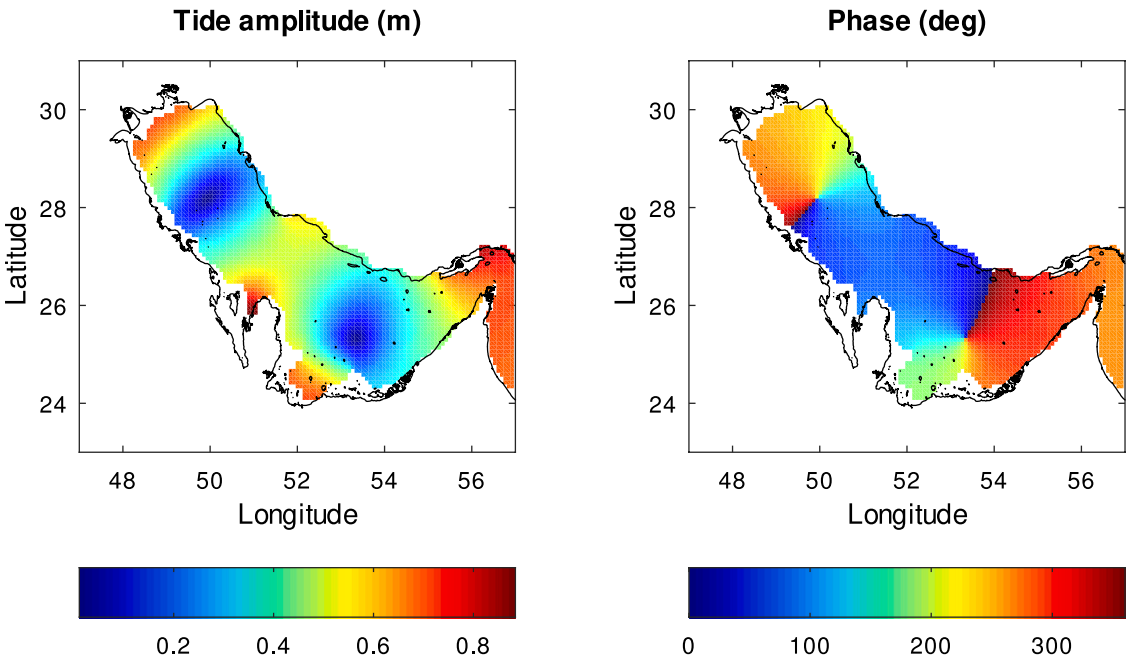

Fig. 4. Calculated chart for the M_2 tide. Phases are given with respect to the local time meridian (adapted phases).

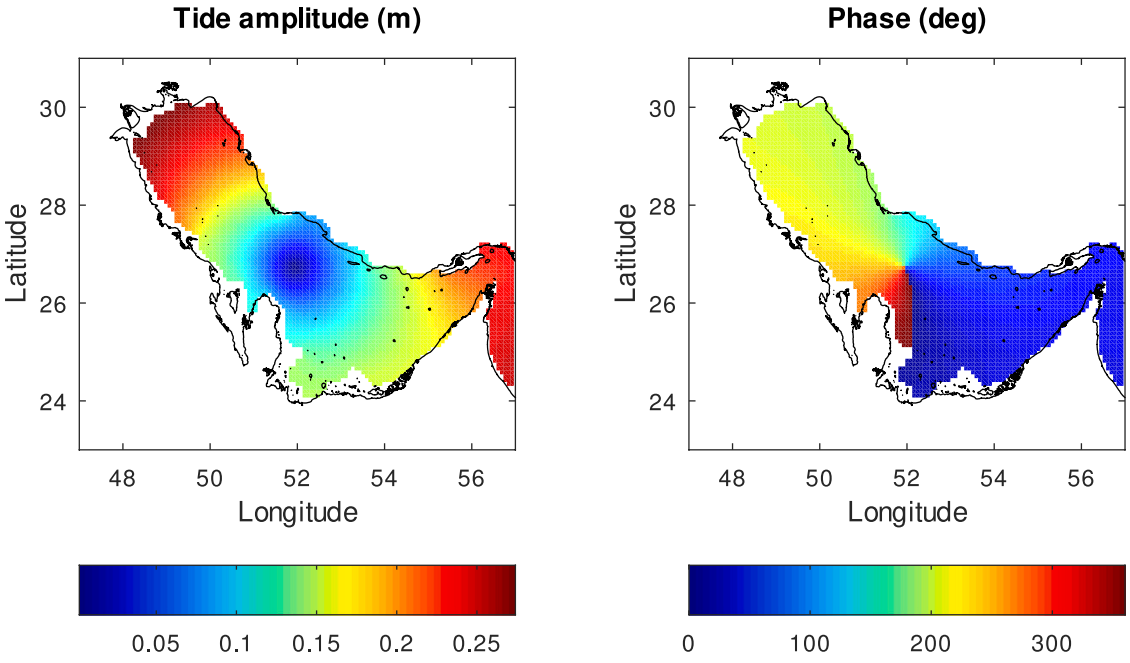

Fig. 5. Calculated chart for the O_1 tide. Phases are given with respect to the local time meridian (adapted phases).

optional and should be included only if a wind forecast is known and it includes unusual weather conditions. Otherwise atmospheric forcing already included in HYCOM calculations is enough for the transport calculations.

2.5. Model output

The model output consists of radionuclide concentrations over the model domain in two water layers: a surface layer whose thickness is defined as 10 m, but can be changed by the user in the code, and a deep layer which extends from the bottom of the surface layer to the seabed. Actually, the model provides the radionuclide inventory in units/m^2 in the deep layer. Concentrations in bed sediments are provided in a 5 cm thick sediment layer. In addition, the model provides the position of particles (both in the water column and in sediments) at the end of the simulation. All this information may be drawn with the Octave scripts which are provided with the model.

A general scheme of the modelling procedure is presented in Fig. 2. All required inputs are in blue boxes. The marine data is pre-computed and does not require any action by the user, which only needs to modify the *release data* and *other*. Once input is defined, the transport code (pink) performs the calculations and provides output (green).

The number of particles used in the model is 200 000. A simulation over three months takes about 10 min on a desktop PC working over Ubuntu 18.04 operating system. All the required codes were written in FORTRAN.

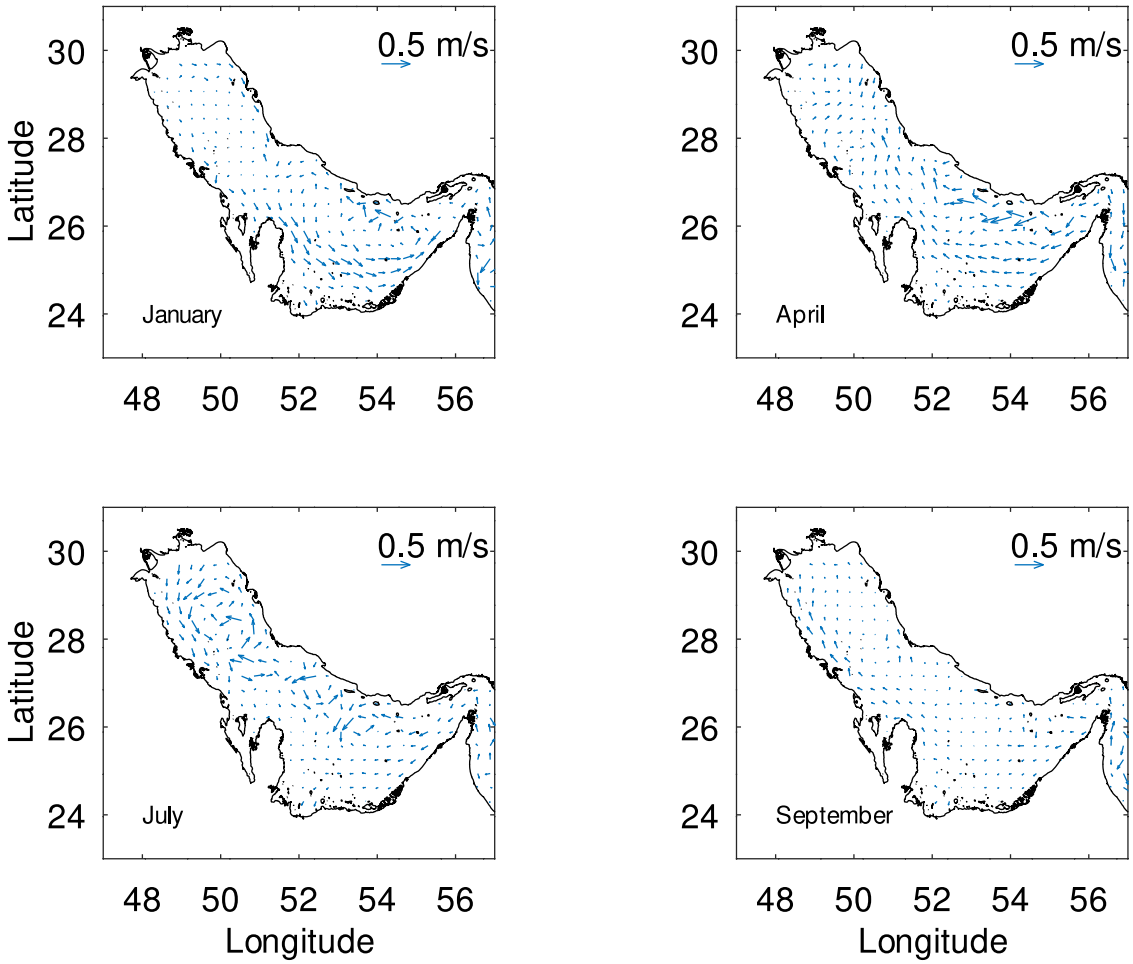

Fig. 6. Water circulation as downloaded from HYCOM model at the end of four months of the year for the sea surface. Only one of each 16 vectors is drawn for more clarity.

3. Results

3.1. Hydrodynamics

The tidal model was calibrated changing the bed friction coefficient until the best agreement between calculated and observed (from Pous et al. (2012)) tidal elevations was achieved. Such agreement was measured as χ^2, according to the equation (Glover et al., 2011):

$$\chi^2 = \frac{1}{N}\sum_{i=1}^{N}\frac{(Z_i^{obs} - Z_i^{cal})^2}{\sigma_i^2} \quad (1)$$

where N is the number of observations, Z_i^{obs} and Z_i^{cal} are observed and calculated elevations respectively, and finally σ_i is the uncertainty in each measurement, taken as 0.01 m according to the observations presented in Pous et al. (2012). A comparison between observed and calculated elevations for the five constituents may be seen in Fig. 3. Although agreement is generally good, there are stations where higher discrepancies appear. Most likely it is due to the relatively coarse resolution of the model: tides where simulated using the same grid as HYCOM, which is 0.08°. Using a finer grid would improve results, but this would be overcome by errors and difficulties in interpolating currents from one grid to the other in order to deal simultaneously with tidal and baroclinic currents.

As a couple of examples, tidal charts for one semidiurnal (M_2) and one diurnal (O_1) tide are respectively presented in Figs. 4 and 5. These charts are in good agreement with earlier calculations made for the APG (Pous et al., 2012; Hyder et al., 2013; Akbari et al., 2016). Thus, in the case of the M_2 tide there are two amphidromes, at (50°E, 28°N) and (53°E, 25°N) approximately. In contrast, diurnal tides show a single one. In case of the O_1 tide it is located approximately at (52°E, 27°N). These locations are in agreement with those presented in Akbari et al. (2016).

Fig. 6 presents a few examples of surface water circulation as calculated by HYCOM model at the end of the indicated months. Circulation is essentially cyclonic in January and anticyclonic in September, showing the well-known surface inflow of Indian Ocean waters along the Iranian coast (Johns et al., 2003). A cyclonic eddy is also apparent in the northern part in July. Actually, it was found, through numerical simulations, that in summer the north-westward coastal current flowing along Iran evolves into a series of mesoscale anticyclonic eddies with typical diameter about 120 km. One of these eddies was apparent in the northern region of the Gulf (Thoppil and Hogan, 2010).

3.2. Radionuclide dispersion

The model can be applied to any radionuclide, simply using its specific distribution coefficient and radioactive decay constant. Here we present some examples with ^{137}Cs and ^{239,240}Pu, which have very different geochemical behaviours: the first is quite conservative while plutonium presents a high affinity to be fixed to sediment particles. A summary of model runs which were carried out is presented in Table 3.

An hypothetical accident occurring at Bushehr NPP (coordinates 50.88° E, 28.82° N) was simulated. A ^{137}Cs release was supposed to last 90 days, with a total activity released equal to 1 PBq. This is just an example, but it is the same order of magnitude as the direct release from Fukushima into the Pacific Ocean during the first three months after the

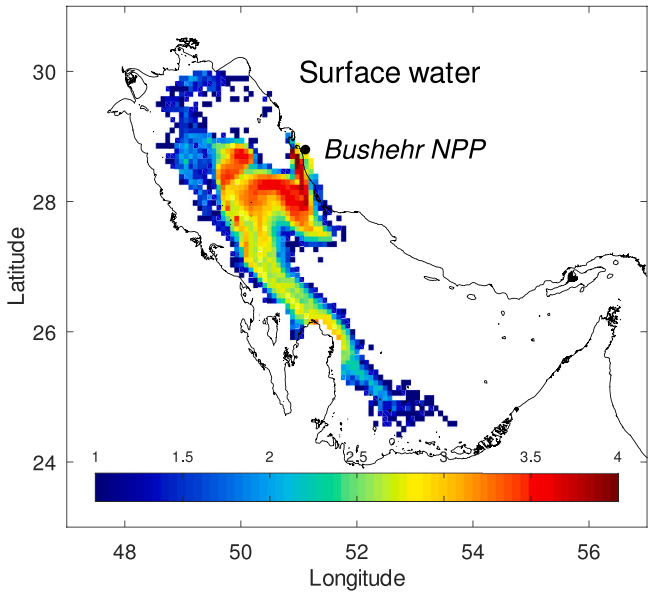

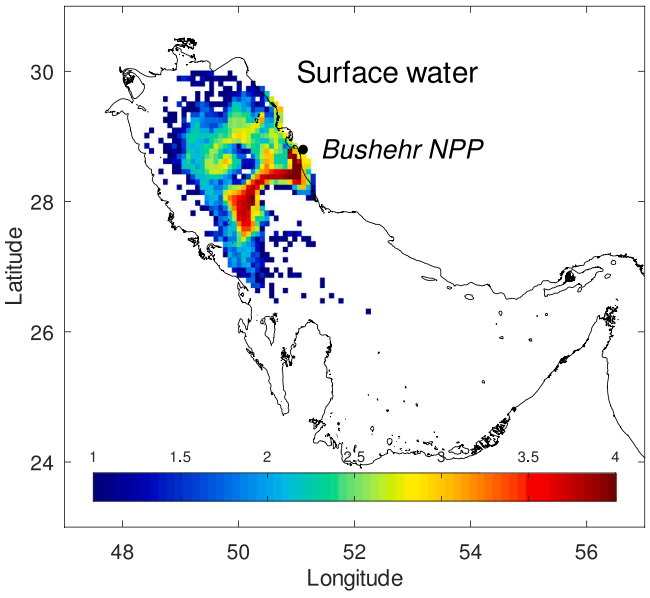

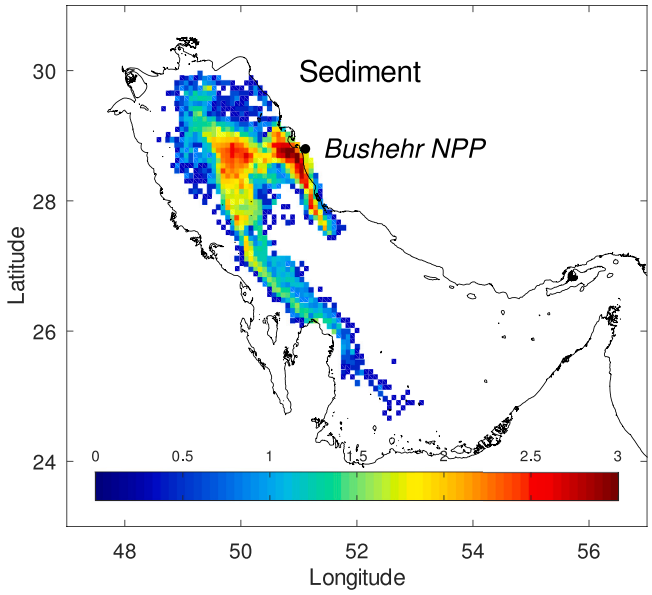

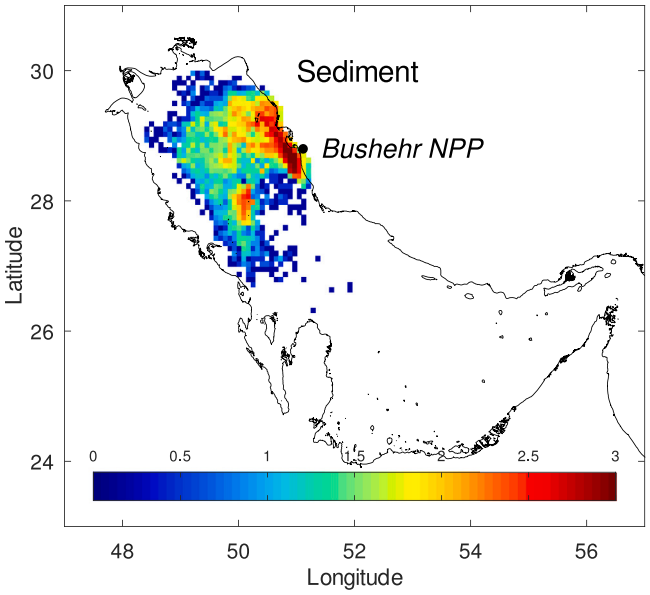

Fig. 7. ^{137}Cs concentrations (logarithmic scale) in surface water (Bq/m^3) and bed sediments (Bq/kg) after 90 days of a release starting in March 21 in Bushehr NPP (run 1). Details of the hypothetical accident are given in the text.

Fig. 8. ^{137}Cs concentrations (logarithmic scale) in surface water (Bq/m^3) and bed sediments (Bq/kg) after 90 days of a release starting in June 21 (run 2). Details of the hypothetical accident are given in the text.

Table 3
Summary of model runs. Starting time of the releases was 12:00 h local time in all cases (year 2021). Local wind was not included in any case and all tidal constituents and residuals were considered. Release magnitude was 1 PBq during 90 days in all runs.

	Radionuclide	Location	Simulated time	Starting time
Run 1	^{137}Cs	Bushehr NPP	90 days	March 21
Run 2	^{137}Cs	Bushehr NPP	90 days	June 21
Run 3	^{137}Cs	Bushehr NPP	90 days	September 21
Run 4	^{137}Cs	Bushehr NPP	90 days	December 21
Run 5	^{137}Cs	Bushehr NPP	1 year	March 21
Run 6	^{239,240}Pu	Bushehr NPP	90 days	March 21
Run 7	^{137}Cs	Barakah NPP	90 days	March 21

2011 tsunami (Kobayashi et al., 2013). The ^{137}Cs k_d was fixed as 4.0 m^3/kg, which is the established value for coastal waters by IAEA (2004) and radioactive decay constant for this radionuclide is 7.29×10^{-10} s^{-1} (half life of 30.17 year). The release was supposed to occur at the sea surface and simulation time was 90 days. Four simulations were carried out with different starting times: 21 March, 21 June, 21 September and 21 December. All releases were finally supported to start at 12:00 h local time. The optional local winds are not included in these calculations, but only the atmospheric forcing already described within HYCOM model. The five tidal constituents and their residuals were included (all switches in file `input.dat` set to 1). The simulations shown as examples are relatively long (90 days) simply to illustrate general transport patterns in the APG. In the case of an accident it may be relevant to carry out short term (few days) simulations to support decision-making and undertake preventing actions in the region around the accident.

Maps of ^{137}Cs in surface water, taken as a 10 m thick layer, and bed sediments after the simulations were obtained, which are presented in Figs. 7 to 10. It seems clear that the starting time of the release

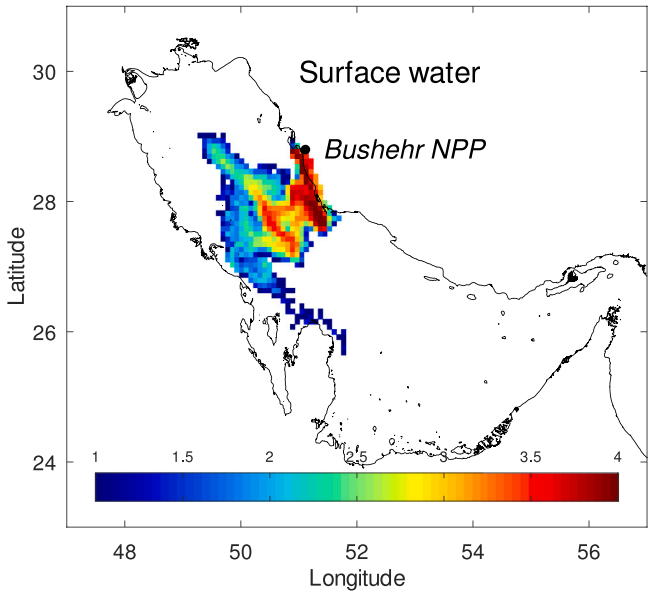

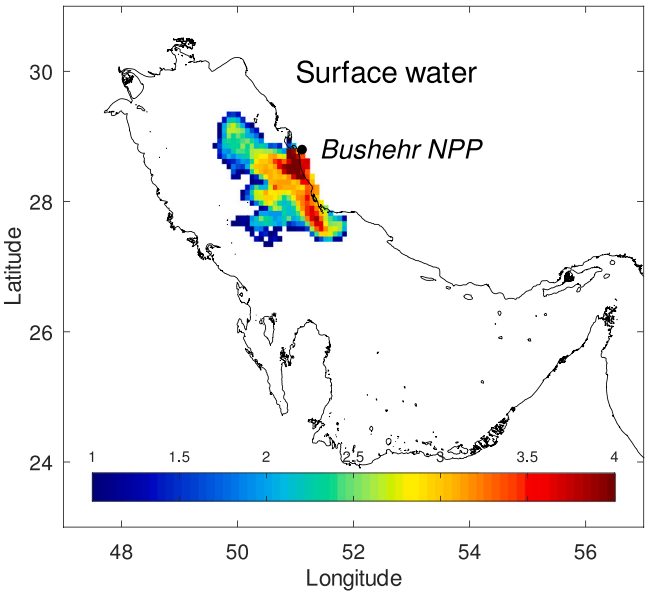

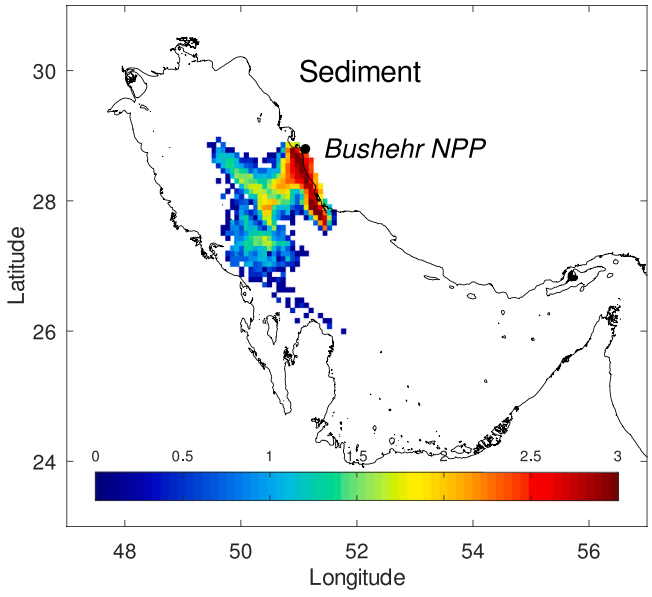

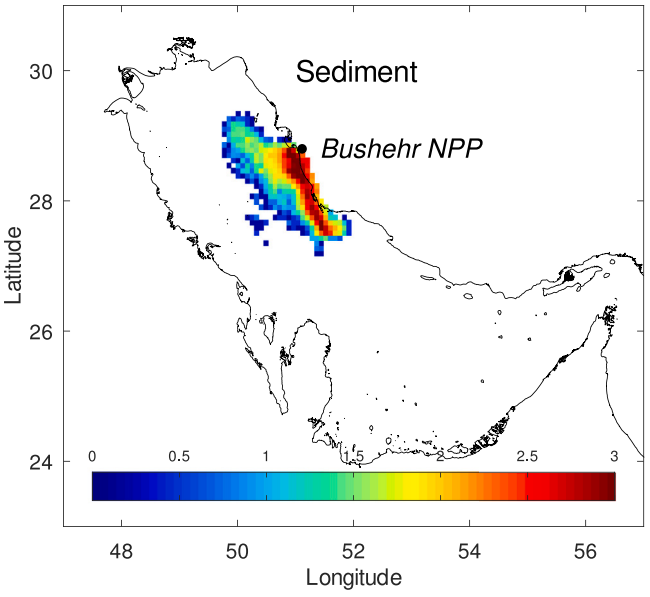

Fig. 9. ^{137}Cs concentrations (logarithmic scale) in surface water (Bq/m^3) and bed sediments (Bq/kg) after 90 days of a release starting in September 21 (run 3). Details of the hypothetical accident are given in the text.

Fig. 10. ^{137}Cs concentrations (logarithmic scale) in surface water (Bq/m^3) and bed sediments (Bq/kg) after 90 days of a release starting in December 21 (run 4). Details of the hypothetical accident are given in the text.

affects the subsequent radionuclide distributions due to the temporal variability of baroclinic circulation. Thus, if the release starts with spring (Fig. 7) radionuclides move to the north and to the central APG, then travelling to the south along the western side. Sediments are contaminated as waters containing ^{137}Cs move over them. Since the water/sediment interaction model is dynamic, sediments buffer radionuclides which are later released as water above them is cleaned. Thus, the concentration map for surface water is an instantaneous picture of the radionuclide distribution at exactly that time; but the map for sediments integrate the whole path followed by the release.

If the release starts with summer (Fig. 8), the sediment map indicates that transport has been predominantly directed to the north, while it is directed to the south if the release starts with fall (Fig. 9). In this case there is also some transport to the south along the western side, as in Fig. 7. Finally, if the release starts with winter (Fig. 10) radionuclides remain close to Bushehr NPP; transport is mainly directed to the south along the Iranian coast and radionuclides do not reach the western coast of the APG in the simulated temporal frame.

As a conclusion, it seems evident that the moment when an accident occurs determines the fate of the released radionuclides and the portion of the APG coast which is potentially contaminated. However, the four simulations show that radionuclides do not reach the north extreme of the APG. It can be probably attributed to the freshwater input from Shatt Al Arab river (Tigris and Eufrates) at the Gulf head, although it should be noted that the present day inflow is much smaller than it once was because of dam projects in Turkey (Hyder et al., 2013).

The accident starting in March (Fig. 7) has been simulated during one year and results are presented in Fig. 11; where ^{137}Cs concentrations in surface water, bed sediment and inventory of radionuclides in the bottom water layer (from 10 m depth to the seabed), in Bq/m^2, may be seen. If the simulation time is extended, a significant amount of radionuclides reach the bottom water layer and are able to contaminate

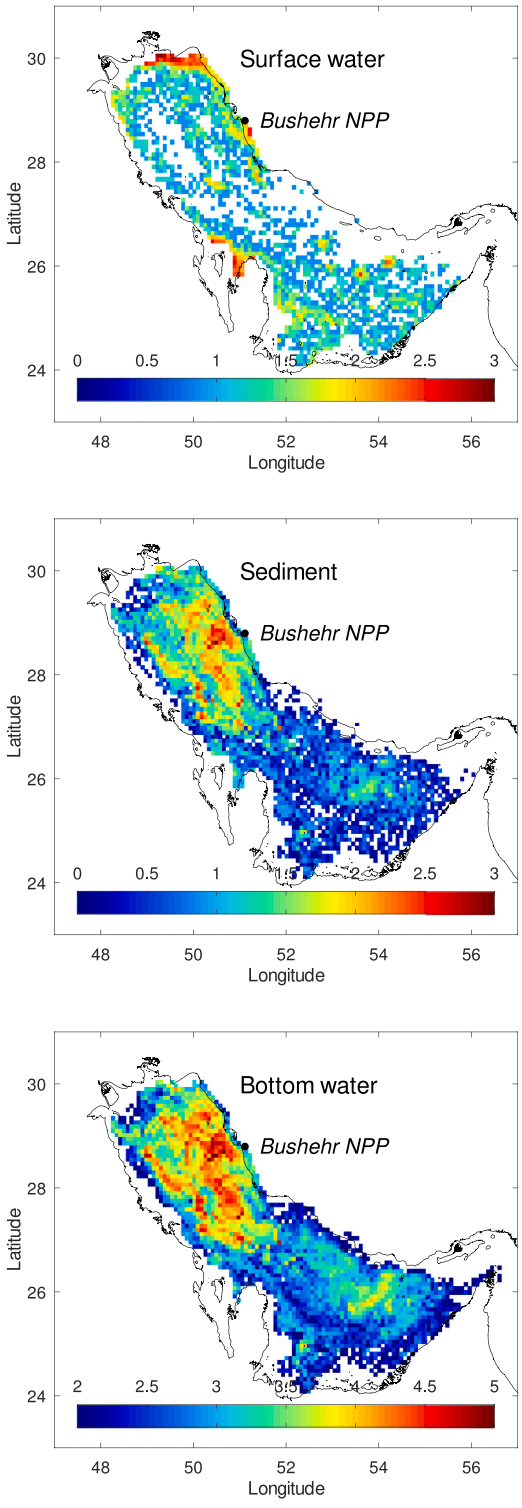

Fig. 11. Same as Fig. 7 but for a one year long simulation (run 5). Inventory (Bq/m^2) of ^{137}Cs in the bottom water layer is also shown. Note the different colour scales for waters. Details of the hypothetical accident are given in the text.

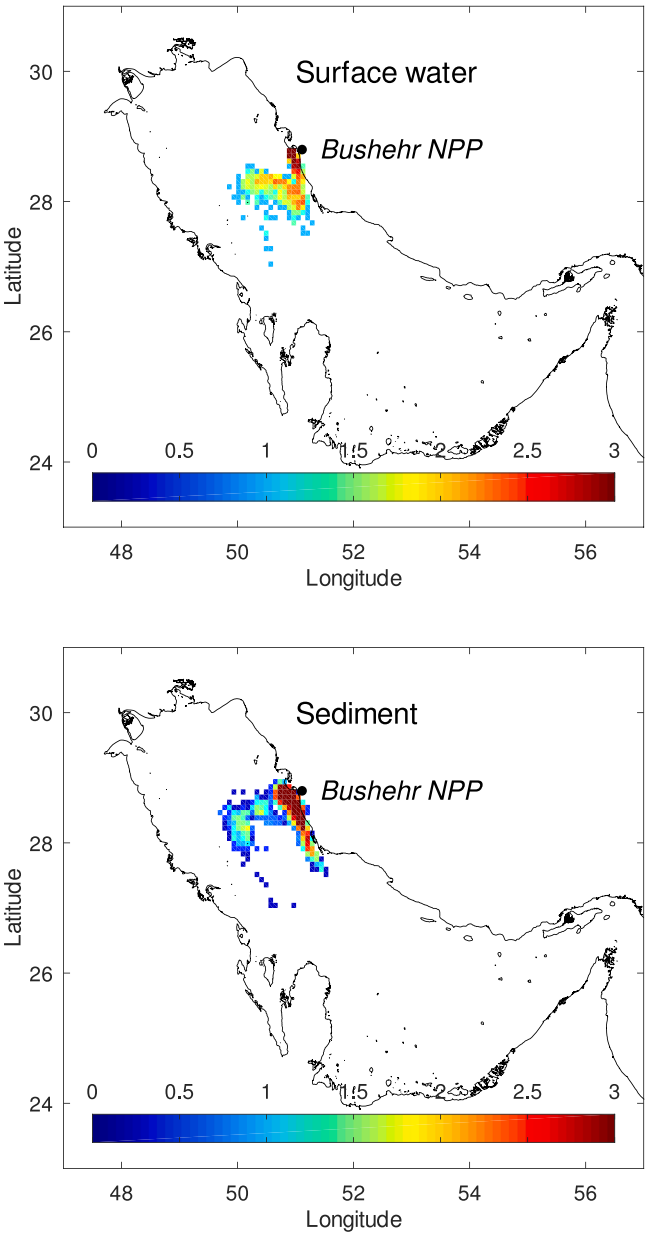

Fig. 12. ^{239,240}Pu concentrations (logarithmic scale) in surface water (Bq/m^3) and bed sediments (Bq/kg) after 90 days of a release starting in March 21 (run 6). Details of the hypothetical accident are given in the text.

the bed sediments. Actually, virtually all the sediments of the APG contain ^{137}Cs (Fig. 11). Radionuclides in the bottom water layer reach the Strait of Hormuz, travelling with the deep outflow water, and will leave the APG entering the Gulf of Oman.

The geochemical behaviour of the radionuclide affects the fate of the release. For instance, the experiment shown in Fig. 7 was repeated but supposing that the released radionuclide was ^{239,240}Pu, whose recommended k_d value is 100 m^3/kg according to IAEA (2004). Thus, it is much more reactive than ^{137}Cs, presenting a higher affinity to be fixed to the sediment. This can be clearly seen comparing Fig. 12, which shows the plutonium results, with the previous Fig. 7: ^{239,240}Pu is quickly fixed to the sediments in the release area, thus presents low mobility in a shallow marine environment like the APG is.

As a final example, exactly the same accident as shown in Fig. 7 was simulated for ^{137}Cs but occurring in Barakah NPP (coordinates 52.23° E, 23.97° N) in UAE. Thus, details on the release are presented above. Concentrations resulting from this Barakah NPP release can be seen in Fig. 13. In this case the released ^{137}Cs moves towards the Strait of Hormuz, but currents in this region of the APG are weaker and the extension of the contaminated area is much smaller than for the previous simulation.

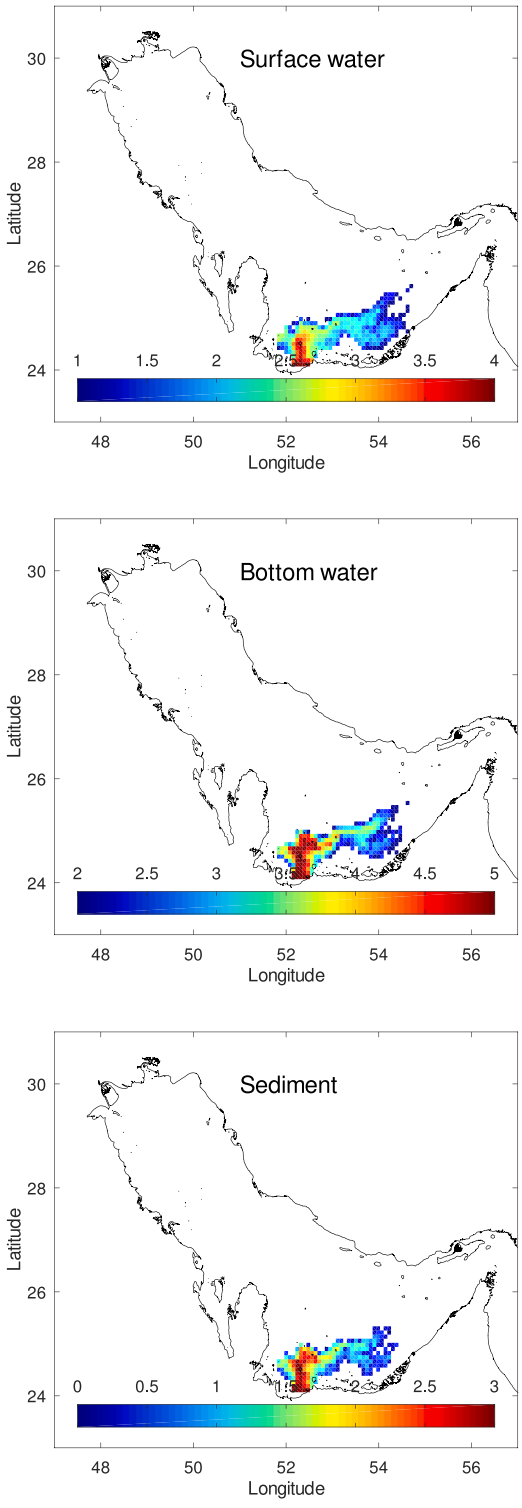

Fig. 13. ^{137}Cs concentrations (logarithmic scale) in surface water (Bq/m^3), inventory in the deep layer (Bq/m^2) and concentration in bed sediments (Bq/kg) for a release occurring in Barakah NPP (run 7). Details of the hypothetical accident are given in the text.

4. Conclusions

A model which simulates the transport of radionuclides in the Arabian/Persian Gulf was presented. The model is Lagrangian and includes physical transport (advection by currents and diffusion due to turbulence) plus radioactive decay and radionuclide interactions with sediments. These processes are described in a dynamic way using a stochastic method. Tidal currents are obtained from a tide model which is run and tested in advance; then tidal analysis is carried out and tidal constants are stored in files which are later read by the transport model. Thus, the tidal state at any time and position is obtained. Baroclinic currents were downloaded from the well-known HYCOM ocean model.

The transport model is easy to setup for any situation since just requires the modification of a few input files specifying the radionuclide and release characteristics. Running times are short (a few minutes for a several day long simulation) even on a desktop PC, which makes it appropriate for a rapid assessment of a hypothetical accident occurring in the APG.

Some examples of radionuclide releases were simulated to illustrate the functioning of the model. However, it was interesting to find that even for a relatively long accident (three months), the moment when releases start will affect the fate of the discharged radionuclides due to the variability of baroclinic currents. As occurs in the Red Sea (Periáñez, 2020a), the relevance of tides depends on the area of the accident since tidal currents increase in straits and also depend on the location of amphidromes. As shown in Section 3.1 tides are significant in the APG and should be described within a transport model. Finally, results for Cs and Pu are very different due to the different geochemical behaviours of these radionuclides: Pu is very reactive, thus it is quickly fixed to bed sediments and presents a low mobility in a shallow marine environment, in comparison with Cs. Consequently, it is essential to include water/sediment interactions in marine radionuclide transport models if they are to be applied to some radionuclides.

The present model only provides radionuclide concentrations in abiotic compartments (surface and deep waters and sediments). A further step would be to incorporate a foodweb model which could describe the adsorption of radionuclides by fish. Advances in this topic are described in Maderich et al. (2014); Vives i Batlle et al. (2016) and de With et al. (2021).

Declaration of competing interest

The authors declare that they have no known competing financial interests or personal relationships that could have appeared to influence the work reported in this paper.

Acknowledgement

This work was partially supported by the Spanish Ministerio de Ciencia, Innovación y Universidades project PGC2018-094546-B-I00 and Junta de Andalucía (Consejería de Economía y Conocimiento), Spain project US-1263369.

Appendix A. Tidal model equations

The 2D depth-averaged barotropic hydrodynamic equations describing tide propagation are the following [see for instance (Kowalik and Murty, 1993)]:

$$\frac{\partial \zeta}{\partial t} + \frac{\partial}{\partial x}(Hu) + \frac{\partial}{\partial y}(Hv) = 0; \tag{2}$$

$$\frac{\partial u}{\partial t} + u\frac{\partial u}{\partial x} + v\frac{\partial u}{\partial y} + g\frac{\partial \zeta}{\partial x} - \Omega v + \frac{\tau_u}{\rho H} = A\left(\frac{\partial^2 u}{\partial x^2} + \frac{\partial^2 u}{\partial y^2}\right); \tag{3}$$

$$\frac{\partial v}{\partial t} + u\frac{\partial v}{\partial x} + v\frac{\partial v}{\partial y} + g\frac{\partial \zeta}{\partial y} + \Omega u + \frac{\tau_v}{\rho H} = A\left(\frac{\partial^2 v}{\partial x^2} + \frac{\partial^2 v}{\partial y^2}\right), \tag{4}$$

where u and v are the depth averaged water velocities along the x and y axis respectively, h is the undisturbed water depth, ζ is the displacement of the water surface with respect to the mean sea level, due to tides, measured upwards, $H = h+\zeta$ is the total water depth, Ω is the Coriolis parameter ($\Omega = 2\omega \sin\lambda$, where ω is the rotational angular velocity of the Earth and λ is latitude), g is gravity acceleration, ρ is seawater density and A is the horizontal eddy viscosity. τ_u and τ_v are

friction stresses written, as usual, in terms of the following quadratic law:

$$\begin{aligned} \tau_u &= k\rho u\sqrt{u^2+v^2}; \\ \tau_v &= k\rho v\sqrt{u^2+v^2}, \end{aligned} \tag{5}$$

where k is the bed friction coefficient, set after calibration.

All the equations were solved using explicit finite difference schemes (Kowalik and Murty, 1993) with second order accuracy. Particularly, the MSOU (Monotonic Second Order Upstream) was used for non-linear terms in the momentum equations. Time step was fixed as 20 s to ensure numerical stability. As mentioned in the main body of the paper, measurements in Pous et al. (2012) were used as open boundary conditions.

Tidal sea surface elevation for the corresponding instant of time t at a given location, $Z(t)$, is obtained from the calculated tidal amplitudes and phases using the tidal prediction equation, which is (Parker, 2007; Boon, 2011):

$$Z(t) = H_0 + \sum_{i=1}^{5} G_i f_i \cos(w_i t - g_i + V_i) \tag{6}$$

where H_0 is the location datum, w_i is frequency of constituent i, G_i and g_i are amplitude and phase (adapted phase, i.e., for the local time meridian) for the corresponding location (these quantities are obtained from the tidal analysis), f_i is nodal factor and V_i the equilibrium argument of the constituent at Greenwich. Note that the sum extends to 5 since this is the number of included constituents. Nodal factors and equilibrium arguments for year 2021 are used. This implies that $t = 0$ is at the beginning of this year, although values for any other year may be used. As usual in this type of models (Proctor et al., 1994; Elliott et al., 2001; Periáñez and Pascual-Granged, 2008) the same treatment is given to tidal currents.

The tidal residual current is evaluated from the following equation (Delhez, 1996):

$$\vec{q}_r = \frac{\langle \vec{q}H \rangle}{\langle H \rangle} \tag{7}$$

where $\vec{q}_r$ is the residual current vector (actually evaluated as a tidal residual transport), $\vec{q}$ is the instantaneous tidal velocity vector and $\langle\rangle$ means time averaging over a tidal cycle.

Appendix B. Lagrangian transport model equations

Advection in a Lagrangian model is computed solving the following equation for each particle:

$$\Delta x = U\,\Delta t + \frac{\partial K_h}{\partial x}\Delta t \tag{8}$$

$$\Delta y = V\,\Delta t + \frac{\partial K_h}{\partial y}\Delta t \tag{9}$$

where Δx and Δy are the changes in particle position (x, y); U and U are water velocity components at the particle position and depth and for the corresponding calculation time step, since currents change in time. These currents are the simple addition of baroclinic currents (downloaded from HYCOM model) and tidal currents and residuals derived from the tidal model described in Appendix A, since both models run over the same computational grid. Note that daily HYCOM currents are used for the baroclinic ones while tidal currents are deduced from analytical functions in the form of Eq. (6) as explained in Appendix A.

Derivatives of the horizontal diffusion coefficient (K_h) prevent the artificial accumulation of particles in regions were diffusion coefficients are lower (Proehl et al., 2005). Nevertheless, these terms are not relevant here since uniform values for K_h are used in this model. Actually, a value equal to 10 m^2/s (the same as horizontal eddy viscosity in the tidal model) was used. The use of constant diffusivities is just a simplification to speed up calculations, although more complex descriptions could be implemented. An example is the Smagorinsky scheme (Cushman-Roisin and Beckers, 2011). Actually, several Lagrangian radionuclide transport models were applied to the Pacific Ocean (Periáñez et al., 2019b), some of them with constant and some with Smagorinsky diffusivities, providing very similar results. Moreover, the horizontal diffusivity may be related to the grid spacing according to a standard equation (Periáñez, 2005). Such equation leads to a value equal to 7.4 m^2/s for the 0.08° resolution used in this model. Thus 10 m^2/s is an appropriate value for the present resolution.

A first order accuracy scheme was used to describe advection. Nevertheless, Elliott and Clarke (1998) did not find improvements in results using a second order accuracy scheme. Moreover, turbulence masks small errors in the advection scheme in marine transport processes (Elliott and Clarke, 1998).

The maximum size of the horizontal step given by the particle due to turbulent mixing, D_h, is (Proctor et al., 1994; Periáñez and Elliott, 2002):

$$D_h = \sqrt{12K_h\Delta t} \tag{10}$$

in the direction $\theta = 2\pi RAN$, where RAN is an uniform random number between 0 and 1 and Δt is time step in the Lagrangian model. This equation gives the maximum size of the step. The real size at a given time and for a given particle is obtained multiplying the equation by another independent random number. This procedure is required to ensure that a Fickian diffusion process (Proctor et al., 1994) is simulated. Time step used to integrate the Lagrangian model was set as $\Delta t = 600$ s.

Similarly, the size of the vertical step is (Proctor et al., 1994; Periáñez and Elliott, 2002):

$$D_v = \sqrt{2K_v\Delta t} \tag{11}$$

given either upward or downward. K_v is the vertical diffusion coefficient, set as 1.0×10^{-5} m^2/s (Elliott et al., 2001).

Radioactive decay is solved with a stochastic method (Periáñez and Elliott, 2002). Decay probability is defined as:

$$p_d = 1 - e^{-\lambda\Delta t} \tag{12}$$

where λ is the radioactive decay constant. A new random number is generated. If $RAN \le p_d$ the particle decays and is removed from the computation.

A stochastic method is also applied to describe interactions between dissolved radionuclides and the bed sediments. These interactions are described in terms of a kinetic adsorption rate k_1 and a desorption rate k_2 (Section 2.3). The probability that a dissolved particle is adsorbed by the sediment is:

$$p_a = 1 - e^{-k_1\Delta t} \tag{13}$$

If a new generated independent random number is $RAN \le p_a$, then the particle is adsorbed by the sediment. The probability that a particle which is fixed to the sediment is redissolved is written as:

$$p_r = 1 - e^{-k_2\phi\Delta t} \tag{14}$$

and the same procedure follows. ϕ is a correction factor that takes into account that part of the sediment surface is hidden by surrounding sediments. Thus, this part is not interacting with water.

The number of units corresponding to each particle, R is deduced from the number of particles in the simulation ($NP = 200\,000$ as mentioned in Section 2.5) and the magnitude of the release M:

$$R = \frac{M}{NP} \tag{15}$$

Then the concentration of radionuclides in the surface water layer of each grid cell $C_{surf}(i,j)$ is:

$$C_{surf}(i,j) = \frac{RN_{surf}(i,j)}{\Delta x\Delta y d_{pic}} \tag{16}$$

where $\Delta x \Delta y$ gives the cell surface, $N_{surf}(i,j)$ is the number of particles in the surface layer of cell (i,j) and d_{pic} is the surface layer thickness (thus we consider only particles at depth less than d_{pic}). The radionuclide inventory in the deep water layer is given by:

$$I_{deep} = \frac{RN_{deep}(i,j)}{\Delta x \Delta y} \quad (17)$$

where $N_{deep}(i,j)$ is the number of particles in cell (i,j) at depth larger than d_{pic}. Finally, radionuclide concentration in the bed sediment of cell (i,j) is:

$$C_{sed}(i,j) = \frac{RN_{deep}(i,j)}{\Delta x \Delta y L \rho_s} \quad (18)$$

where $N_{sed}(i,j)$ is the number of particles in the bed sediment of cell (i,j), L is sediment thickness (set as 0.05 m as mentioned in Section 2.5) and ρ_s is sediment bulk density:

$$\rho_s = \rho_m(1 - por) \quad (19)$$

where $\rho_m = 2600\ \mathrm{kg/m^3}$ is mineral particle density and por is sediment porosity. A number of parameters are defined within the code, whose values are selected from standard ones or previous works. Thus, porosity is set as $por = 0.6$, the desorption kinetic rate as $k_2 = 1.16 \times 10^{-5}\ \mathrm{s^{-1}}$, the sediment correction factor as $\phi = 0.1$ and the water surface layer thickness as $d_{pic} = 10$ m. Of course, these values may be changed if desired.

References

Abdi, M.R., Faghihian, H., Kamali, M., Mostajaboddavati, M., Hasanzadeh, A., 2006. Distribution of natural radionuclides on coasts of Bushehr, Persian Gulf, Iran. Iran. J. Sci. Technol. Trans. A 30 (A3), 259–269.

Akbari, P., Sadrinasab, M., Chegini, V., Siadatmousavi, M., 2016. Tidal constituents in the Persian Gulf, Gulf of Oman and Arabian Sea: a numerical study. Indian J. Geo-Marine Sci. 45 (8), 1010–1016.

Al-Ghamdi, H., Al-Muqrin, A., El-Sharkawy, A., 2016. Assessment of natural radioactivity and ^{137}Cs in some coastal areas of the Saudi Arabian gulf. Mar. Pollut. Bull. 104, 29–33.

Al-Rabeh, A.H., Lardner, R.W., Gunay, N., 2000. Gulfspill version 2.0: a software package for oil spills in the Arabian Gulf. Environ. Model. Softw. 15, 425–442.

Alosairi, Y., Pokavanich, T., 2017. Seasonal circulation assessments of the Northern Arabian/Persian Gulf. Mar. Pollut. Bull. 116, 270–290.

Batlle, J.Vives.i., Beresford, N., Beaugelin-Seiller, K., Bezhenar, R., Brown, J., Cujic, M.Jing-Jy.Cheng., Dragovic, S.S., Duffa, C., Fievet, B., Hosseini, A., Jung, K.T., Kamboj, S., Kobayashi, T.Dong-Kwon.Keum., Kryshev, A., Poire, D.Le., Maderich, V., Periáñez, R.Byung.Il.Min., Sazykina, T., Suh, K.S., Yu, C., Wang, C., Heling, R., 2016. Inter-comparison of dynamic models for radionuclide transfer to marine biota in a fukushima accident scenario. J. Environ. Radioact. 153, 31–50.

Bleck, R., 2001. An oceanic general circulation model framed in hybrid isopycnic-Cartesian coordinates. Ocean Model. 4, 55–88.

Boon, J.D., 2011. Secrets of the Tide. Woodhead Publishing, USA.

Cushman-Roisin, B., Beckers, J.M., 2011. Introduction To Geophysical Fluid Dynamics. Elsevier.

de With, G., Bezhenar, V., Maderich, Y., Yevdin, M., Iosjpe, F., Qiao, R., Periáñez, R., 2021. Development of a dynamic food chain model for assessment of the radiological impact from radioactive releases to the aquatic environment. J. Environ. Radioact. 233, 106615.

Delhez, E.J.M., 1996. On the residual advection of passive constituents. J. Mar. Syst. 8, 147–169.

Elliott, A.J., Clarke, S., 1998. Shallow water tides in the firth of forth. Hydrograph. J. 87, 19–24.

Elliott, A.J., Wilkins, B.T., Mansfield, P., 2001. On the disposal of contaminated milk in coastal waters. Mar. Pollut. Bull. 42, 927–934.

Environmental Agency Abu Dhabi, 2009. Abu Dhabi Water Resources Master Plan. Environmental Agency Abu Dhabi, Abu Dhabi.

Faghihifard, M., Badri, M.A., 2016. Simulation of oil pollution in the Persian Gulf near Assaluyeh oil terminal. Mar. Pollut. Bull. 105, 143–149.

Glover, D.M., Jenkins, W.J., Doney, S.C., 2011. Modeling Methods for Marine Science. Jenkins, W, J Doney, S.C Cambridge University Press, UK.

Hassanvand, M., Mirnejad, Z., 2019. Hydrodynamic model of radionuclide dispersion during normal operation and accident of Bushehr nuclear power plant. Prog. Nucl. Energy 116, 115–123.

Hyder, P., While, J., Arnold, A., O'Dea, E., Furner, R., Siddorn, J., Martin, M., Sykes, P., 2013. Evaluating a new NEMO-based Persian/Arabian Gulf tidal operational model. J. Oper. Oceanograph. 6 (1), 3–16.

IAEA, 2001. Generic Models For Use In Assessing The Impact Of Discharges Of Radioactive Substances To The Environment. Safety Reports Series 19, Vienna.

IAEA, 2004. Sediment Distribution Coefficients and Concentration Factors for Biota in the Marine Environment. Technical Reports Series 422, Vienna.

IAEA, 2019. Modelling Of Marine Dispersion And Transfer Of Radionuclides Accidentally Released From Land Based Facilities. IAEA-TECDOC-1876, Vienna.

Johns, W.E., Yao, F., Olson, D.B., Josey, S.A., Grist, J.P., Smeed, D.A., 2003. Observations of seasonal exchange through the Straits of Hormuz and the inferred freshwater budgets of the Persian Gulf. J. Geophys. Res. 108 (C12), 3391. http://dx.doi.org/10.1029/2003JC001881.

Kämpf, J., Sadrinasab, M., 2006. The circulation of the Persian Gulf: a numerical study. Ocean Sci. 2, 27–41.

Kamyab, A., Azad, M.T., Sadeghi, M., Akhound, A., 2018. Dispersion simulation of cesium-137 released from a hypothetical accident at the Bushehr nuclear power plant in Persian Gulf. Int. J. Coastal Offshore Eng. 2 (3), 13–17.

Kobayashi, T., Nagai, H., Chino, M., Kawamura, H., 2013. Source term estimation of atmospheric release due to the Fukushima Dai-ichi Nuclear Power Plant accident by atmospheric and oceanic dispersion simulations. J. Nucl. Sci. Technol. 50, 255–264.

Kobayashi, T., Otosaka, S., Togawa, O., Hayashi, K., 2007. Development of a non-conservative radionuclide dispersion model in the ocean and its application to surface cesium-137 dispersion in the Irish Sea. J. Nucl. Sci. Technol. 44, 238–247.

Kowalik, Z., Murty, T.S., 1993. Numerical Modelling of Ocean Dynamics. World Scientific, Singapore.

Maderich, V., Bezhenar, R., Heling, R., With, G.de., Jung, K.T., Myoung, J.G., Cho, Y.K., Qiao, F., Robertson, L., 2014. Regional long-term model of radioactivity dispersion and fate in the northwestern Pacific and adjacent seas: application to the Fukushima Dai-ichi accident. J. Environ. Radioact. 131, 4–18.

Parker, B.B., 2007. Tidal Analysis and Prediction. NOAA Special Publication NOS CO-OPS 3.

Periáñez, R., 2005. Modelling the Dispersion of Radionuclides in the Marine Environment. an Introduction. Springer.

Periáñez, R., 2007. Chemical and oil spill rapid response modelling in the Strait of Gibraltar-Alborán Sea. Ecol. Model. 207, 210–222.

Periáñez, R., 2009. Environmental modelling in the Gulf of Cadiz: heavy metal distributions in water and sediments. Sci. Total Environ. 407, 3392–3406.

Periáñez, R., 2012. Modelling the environmental behavior of pollutants in Algeciras Bay (south Spain). Mar. Pollut. Bull. 64, 221–232.

Periáñez, R., 2020a. A Lagrangian oil spill transport model for the Red Sea. Ocean Eng. http://dx.doi.org/10.1016/j.oceaneng.2020.107953.

Periáñez, R., 2020b. Models for predicting the transport of radionuclides in the red sea. J. Environ. Radioact. http://dx.doi.org/10.1016/j.jenvrad.2020.106396.

Periáñez, R., Abril, J.M., 2014. A numerical modelling study on oceanographic conditions in the former Gulf of Tartessos (SW Iberia): tides and tsunami propagation. J. Mar. Syst. 139, 68–78.

Periáñez, R., Bezhenar, R., Brovchenko, I., Duffa, C., Iosjpe, M., Jung, K.T., Kobayashi, T., Liptak, L., Little, A., Maderich, V., Min, B.I., Nies, H., Osvath, I., Suh, K.S., With, G.de., 2019a. Marine radionuclide transport modelling: Recent developments, problems and challenges. Environ. Model. Softw. 122, 104523.

Periáñez, R., Bezhenar, R., Brovchenko, I., Duffa, C., Jung, K.T., Kobayashi, T., Lamego, F., Maderich, V., Min, B.I., Nies, H., Osvath, I., Outola, I., Psaltaki, M., Suh, K.S., With, G.de., 2016a. Modelling of marine radionuclide dispersion in IAEA MODARIA program: lessons learnt from the Baltic Sea and Fukushima scenarios. Sci. Total Environ. 569/570, 594–602.

Periáñez, R., Bezhenar, R., Brovchenko, I., Jung, K.T., Kamidara, Y., Kim, K.O., Kobayashi, T., Maderich, V.Liptak.L:., Min, B.I., Suh, K.S., 2019b. Fukushima ^{137}Cs releases dispersion modelling over the Pacific Ocean. Comparisons of models with water, sediment and biota data. J. Environ. Radioact. 198, 50–63.

Periáñez, R., Elliott, A.J., 2002. A particle tracking method for simulating the dispersion of non conservative radionuclides in coastal waters. J. Environ. Radioact. 58, 13–33.

Periáñez, R., Min, B.I., Suh, K.S., 2021. The transport, effective half-lives and age distributions of radioactive releases in the northern Indian Ocean. Mar. Pollut. Bull. 169, 112587.

Periáñez, R., Pascual-Granged, A., 2008. Modelling surface radioactive, chemical and oil spills in the Strait of Gibraltar. Comput. Geosci. 34, 163–180.

Periáñez, R., Suh, K.S., Min, B.I., 2016b. The behaviour of ^{137}Cs in the North Atlantic Ocean assessed from numerical modelling: Releases from nuclear fuel reprocessing factories, redissolution from contaminated sediments and leakage from dumped nuclear wastes. Mar. Pollut. Bull. 113, 343–361.

Periáñez, R., z, M.Casas-Ruí., Bolí var, J.P., 2013. Tidal circulation, sediment and pollutant transport in Cádiz Bay (SW Spain): a modelling study. Ocean Eng. 69, 60–69.

Pous, S., Carton, X., Lazure, P., 2012. A process study of the tidal circulation in the Persian Gulf. Open J. Marine Sci. 2, 131–140.

Proctor, R., Flather, R.A., Elliott, A.J., 1994. Modelling tides and surface drift in the Arabian Gulf: application to the Gulf oil spill. Cont. Shelf Res. 14, 531–545.

Proehl, J.A., Lynch, D.R., McGuillicuddy, D.J., Ledwell, J.R., 2005. Modeling turbulent dispersion on the North Flank of Georges Bank using Lagrangian particle methods. Cont. Shelf Res. 25, 875–900.

Pugh, D.T., 1987. Tides, Surges and Mean Sea Level. Wiley, Chichester, p. 472.

Thoppil, P.G., Hogan, P.J., 2010. A modeling study of circulation and eddies in the Persian Gulf. J. Phys. Oceanogr. 40 (9), 2122–2134.

Tsabaris, C., Tsiaras, K., Eleftheriou, G., Triantafyllou, G., 2021. ^{137}Cs ocean distribution and fate at East Mediterranean Sea in case of a nuclear accident in Akkuyu Nuclear Power Plant. Prog. Nucl. Energy 139, 103879.

Uddin, S., Fowler, S.W., Behbehani, M., Al-Ghadban, A.N., Swarzenski, P.W., Al-Awadhi, N., 2020. A review of radioactivity in the Gulf region. Mar. Pollut. Bull. 159, 111481.

Yao, F., Johns, W.E., 2010a. A HYCOM modeling study of the Persian Gulf: 1. Model configurations and surface circulation. J. Geophys. Res. 115 (C11017).

Yao, F., Johns, W.E., 2010b. A HYCOM modeling study of the Persian Gulf: 2. Formation and export of Persian Gulf water. J. Geophys. Res. 115 (C11018).